

Crystallization and jamming in narrow fluidized beds

This article may be downloaded for personal use only. Any other use requires prior permission of the author and AIP Publishing. This article appeared in *Phys. Fluids* 32, 083303 (2020) and may be found at <https://doi.org/10.1063/5.0015410>.

Fernando David Cúñez¹ and Erick M. Franklin^{1, a)}

School of Mechanical Engineering, UNICAMP - University of Campinas,

Rua Mendeleev, 200, Campinas, SP, Brazil

(Dated: 5 January 2021)

A fluidized bed is basically a suspension of granular material by an ascending fluid in a tube, and it has a rich dynamics that includes clustering and pattern formation. When the ratio between the tube and grain diameters is small, different behaviors can be induced by high confinement effects. Some unexpected and curious behaviors, that we investigate in this paper, are the crystallization and jamming of grains in liquids with velocities higher than that for incipient fluidization, supposed to maintain the grains fluidized. In our experiments, performed in a vertical tube of transparent material, different grains, water velocities, resting times, and velocity decelerations were used. An analysis of the bed evolution based on image processing shows that, after a decreasing flow that reaches a velocity still higher than that for incipient fluidization, grains become organized in lattice structures of high compactness, where they are trapped though with small fluctuations. These structures are initially localized and grow along time, in a similar manner as happens in phase transitions and glass formation. After a certain time, if the liquid velocity is slightly increased, jamming occurs, with grains being completely blocked and their fluctuation disappearing. We show that different lattice structures appear depending on the grain type. Our results provide new insights into fluidization conditions, glass-like formation and jamming.

^{a)}Electronic mail: franklin@fem.unicamp.br; Corresponding author

I. INTRODUCTION

A fluidized bed is basically a suspension of granular material by an ascending fluid, and it is frequently employed in industry for its high rates of mass and heat transfers between the fluid and solids. From the mechanical point of view, fluidized beds have a rich dynamics, with shocks between grains, slipping, contacts, and shedding of small vortices occurring at the grain scale, and the formation of contact networks, clusters, plugs and other structures at larger scales. The coexistence of a large number of important mechanisms at different scales makes the problem complex, and, depending if the employed fluid is a gas or a liquid, some mechanisms have more or less relative importance. For instance, in the case of solid-liquid fluidized beds (SLFBs), fluid drainage dissipates a considerable amount of energy, shocks transmit less energy (although they are of importance), and virtual mass force may be important¹.

Narrow SLFBs, typically with thickness between 10 to 100 grain diameters, have been studied for their distinct behavior when compared to usual beds²⁻¹⁰. Different instabilities and patterns have been identified for that case, such as the propagation of transverse waves⁷ and bubbles⁸, for instance. In the very narrow case, for which the ratio of the tube diameter D to that of grains d is less than 10, different behaviors are induced by high confinement effects^{1,11}. Cúñez and Franklin¹¹ investigated both experimentally and numerically the structure of a very narrow bed ($D/d = 4.2$), and found the formation of alternating regions of high and low particle fractions, called plugs and bubbles, respectively. They showed, by analyzing the network of contact forces, that those structures are associated with the presence of close walls. The same kind of structure is observed in bidesperse beds¹, their presence being more important as D/d decreases. In the case of water, Cúñez and Franklin¹ showed that the added mass force has an effect of decreasing by roughly 10% the characteristic time of the narrow-bed dynamics.

Goldman and Swinney¹² investigated experimentally the crystallization and jamming in a SLFB with D/d of the order of 100. Crystallization consists in the organization of the bed in a static lattice of high compactness. In this lattice, grains have no macroscopic motion, but maintain small fluctuations, usually referred to as microscopic motion. The reasons for the appearance of crystallization are still not understood, but it occurs more frequently during partial defluidization, i.e., by decreasing the fluid velocity of an already fluidized bed until a velocity slightly above that of minimum fluidization, U_{mf} , is reached. Jamming usually appears when a crystallized bed is forced upwards by submitting it to a fluid velocity slightly higher than that of crystallization.

Goldman and Swinney¹² showed that crystallization occurs during partial defluidization, and that the final state depends on the decreasing rate, mainly because grains sediment for deceleration rates above a threshold value. They showed that bed crystallization has similarities with equilibrium glass transition, one of them being the rate dependence and another one the initially localized solid-like regions that grow along time. They showed also that once crystallization is complete, grains lose their macroscopic motion while preserving the microscopic one, and that if the liquid velocity is slightly increased the system is completely jammed.

Tariot et al.¹³ and Gauthier et al.¹⁴ investigated experimentally the compaction of granular material in a SLFB of rectangular cross section with thickness of $10d$. In the experiments, the authors fluidized the bed and then let the grains settle by turning off the water flow. Afterward, they imposed a water flow and measured the evolution of bed compactness for different water velocities, using two types of flows: a continuous water velocity below U_{mf} , and pulses (bursts) of water below¹⁴ and above^{13,14} U_{mf} . They found a slow increase in bed compactness for both cases, with the compaction of the pulsed cases reaching higher values when compared to that of continuous flow. Gauthier et al.¹⁴ showed that under continuous flow compaction is more effective for velocities approaching U_{mf} , and for pulsed flows compaction is much more effective for velocities above U_{mf} . Finally, Gauthier et al.¹⁴ proposed d/U_{mf} as a timescale and that the time evolution of particle fraction follows a logarithmic law.

Most of previous studies dealing with hindrance of fluidization on narrow or small beds concerned either U_{mf} or compaction/expansion of beds from a macroscopic point of view^{15–18}. For example, Jin et al.¹⁵ investigated the expansion and collapse of beds in a pulsed SLFB by analyzing particle concentrations, while Rao et al.¹⁶ investigated the effects of bed height and diameter on U_{mf} by measuring pressure gradients and using a continuous model (which is suitable for large beds). Li et al.¹⁸ and do Nascimento et al.¹⁷ investigated micro SLFBs, with D of the order of 1 mm and d of the order of 10-100 μm , and found that, given the small scales of grains, hindrances are caused by superficial forces acting on grains, including relatively strong adhesion forces. None of them investigated how grains are organized during compaction, the appearance of crystallization within the bed, its susceptibility to jamming, or the behavior of very narrow beds ($D/d < 5$).

Very few studies were devoted to crystallization and jamming in SLFBs and, although some physical aspects of these processes were investigated previously, many questions remain to be clarified. For instance, the involved scales and the effect of higher confinement remain to be

understood. In the present paper, we investigate experimentally the crystallization and jamming of grains in very narrow SLFBs, where we used $D/d = 4.2$ and $D/d = 3.2$ and different grain densities, water velocities, resting times and velocity decelerations. We show that different confinement and grain types generate distinct lattice structures that are initially localized and grow along time. The present results provide new insights into fluidization conditions, glass-like formation and jamming.

II. EXPERIMENTAL SETUP

The experimental setup consisted of a water tank with a heat exchanger, a centrifugal pump, a flow meter, a flow homogenizer, a 1.2-m-long tube of transparent material (polymethyl methacrylate - PMMA) oriented vertically, and a return line, where water flowed in closed loop following the order just described. The vertical tube was aligned vertically within $\pm 3^\circ$ and had an internal diameter of 25.4 mm. The test section corresponded to 0.65 m in length from the entrance of the tube, and a visual box filled with water was placed around it to minimize parallax distortions. Figure 1 shows the layout of the experimental setup and Fig. 2 shows a photograph of part of the test section.

Controlled grains were settled in the test section, forming a granular bed, and upward water flows were imposed by controlling the rotation of the centrifugal pump, which had a maximum flow capacity of 4100 l/h. The flow homogenizer was a 150-mm-long tube containing packed beads with $d = 6$ mm between fine wire screens and it was placed just upstream the test section. In our tests, water temperatures were within $25^\circ\text{C} \pm 3^\circ\text{C}$.

A camera of complementary metal-oxide-semiconductor (CMOS) type was placed perpendicularly to the test section in order to acquire images of the beds. The camera resolution was of $1920 \text{ px} \times 1080 \text{ px}$ at 60 Hz and it was branched to a computer system that controlled both the camera and the pump rotation. With that, the velocity variations were automated and synchronized with the camera. The camera frequency was set to 30 Hz and the region of interest (ROI) to $1920 \text{ px} \times 211 \text{ px}$ in all our tests. We used a lens of 60 mm focal distance and F2.8 maximum aperture mounted on the camera, and we ended with images where 1 px corresponded to approximately 0.1 mm. Lamps of light emission diode (LED) were branched to a continuous-current source to provide a stable light.

Three different beds were investigated, the first consisting of 400 alumina beads with $d_1 = 6$ mm and $S_1 = \rho_p/\rho_f = 3.69$, the second of 400 glass beads with $d_2 = 6$ mm and $S_2 = \rho_p/\rho_f =$

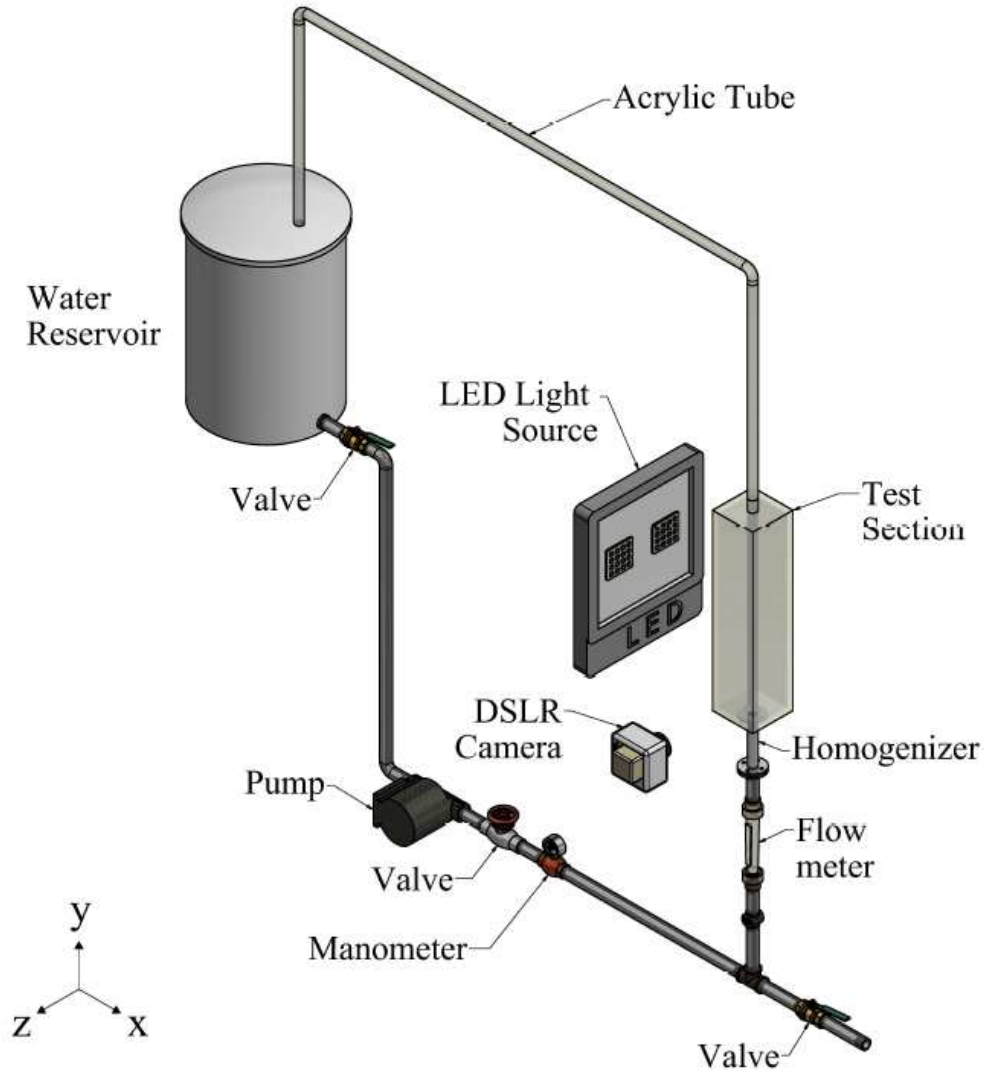


FIG. 1. Layout of the experimental setup.

2.5, and the third of 200 glass beads with $d_3 = 8$ mm and $S_3 = \rho_p/\rho_f = 2.5$, where ρ_p is the density of the bead material and ρ_f the density of the fluid. Microscopy images of the used grains are available in the Supplementary Material. For these beds, the ratios between the tube and grain diameters were of $D/d_1 = 4.2$, $D/d_2 = 4.2$ and $D/d_3 = 3.2$, and the numbers of Stokes $St_t = v_t d \rho_p / (9 \mu_f)$ and Reynolds $Re_t = \rho_f v_t d / \mu_f$ based on terminal velocities, where v_t is the terminal velocity of one single particle and μ_f is the dynamic viscosity of the fluid, are shown in Tab. I. Values of St_t and Re_t in our tests indicate that grains have considerable inertia with respect to the employed fluid. Table I presents also, for the inception of fluidization, the bed heights h_{if} , the particle fraction ϕ_0 , and the settling velocity v_s , the latter computed based on the Richardson–Zaki



FIG. 2. Fluidized bed occupying part of the test section.

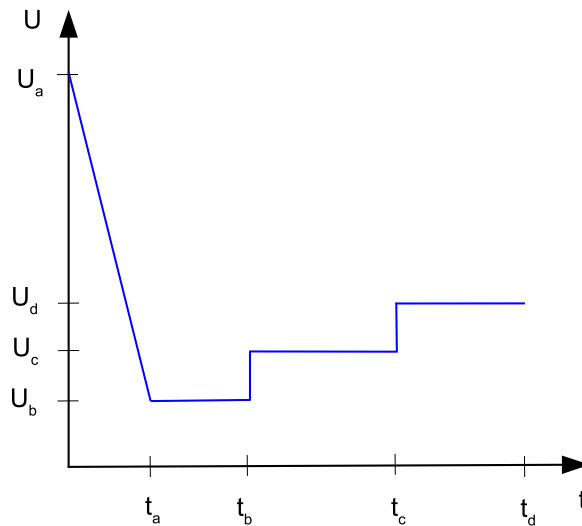


FIG. 3. Scheme of the imposed water velocities along tests. Values are listed in Tabs. I and II.

correlation, $v_s = v_t \phi_0^{2.4}$. Because we had optical access to the bed, we determined the inception of fluidization based on acquired images by detecting the motion of grains and associating the respective water velocity with an incipient fluidization velocity U_{if} . This procedure is different from the usual method for determining U_{mf} based on pressure differences. While, on the one hand, beds consisting of a small number of grains are susceptible to relatively high pressure variations

Crystallization and jamming in narrow fluidized beds

TABLE I. Grain diameter d , particle type, density ratio S , terminal Reynolds number Re_t , terminal Stokes number St_t , bed height at the inception of fluidization h_{if} , particle fraction at the inception of fluidization ϕ_0 , settling velocity v_s , incipient fluidization velocity U_{if} , and velocities U_a, U_b, U_c and U_d normalized by U_{if} .

d	Species	S	Re_t	St_t	h_{if}	ϕ_0	v_s	U_{if}	U_a/U_{if}	U_b/U_{if}	U_c/U_{if}	U_d/U_{if}
mm	m	...	m/s	m/s
6.0	1	3.69	4026	1650	0.174	0.51	0.118	0.118	1.86	1.02	1.07	1.16
6.0	2	2.50	2967	824	0.165	0.54	0.076	0.076	2.89	1.01	1.08	1.37
8.0	3	2.50	4654	1293	0.220	0.48	0.120	0.120	1.83	1.01	1.05	1.14

at the inception of fluidization, on the other hand it is relatively easy to detect the motion of their grains and verify that they are suspended. The values of U_{if} , obtained from image processing and not necessarily equal to U_{mf} , are also shown in Tab. I.

In our tests, we initially fluidized the bed by imposing a cross-sectional mean velocity $U_a = 0.219$ m/s, corresponding to $U_a/U_{if1} = 1.86$, $U_a/U_{if2} = 2.89$ and $U_a/U_{if3} = 1.83$, during 90 s, then we reduced the velocity at a given deceleration rate until reaching a value U_b slightly above that of incipient fluidization (≈ 101 to 102% U_{if}), which was maintained for a certain time. Afterward, we increased the velocity slightly, to U_c around 105 to 108% U_{if} , and maintained it for a given time, and finally we increased it slightly again to U_d around 114 to 137% U_{if} and maintained it for a given time interval. For each grain type, different velocity decelerations and time intervals were used. Figure 3 shows the imposed water velocities, and Tab. I presents the values of velocities and Tab. II the time instants of each test.

TABLE II: Test number, particle type, programmed times t_a, t_b, t_c and t_d , time of the beginning of crystallization t_{cry} , number of times that crystallization occurred N_{cry} , intensity of crystallization $I_{cry} = \Delta t_{cry}/(t_b - t_a)$, number of times that jamming occurred N_{jam} , intensity of jamming $I_{jam} = \Delta t_{jam}/\Delta t_2$, and intensity of the volcano-like structure $I_{vol} = \Delta t_{vol}/\Delta t_3$.

Test	Species	t_a	t_b	t_c	t_d	t_{cry}	N_{cry}	I_{cry}	N_{jam}	I_{jam}	I_{vol}
...	...	s	s	s	s	s
1	1	10	600	1200	1500	485	1	0.19	1	1.00	...
2	1	10	900	1800	2100	830	1	0.08	1	0.61	...

Crystallization and jamming in narrow fluidized beds

Continuation of Table II											
Test	Species	t_a	t_b	t_c	t_d	t_{cry}	N_{cry}	I_{cry}	N_{jam}	I_{jam}	I_{vol}
...	...	s	s	s	s	s
3	1	10	1200	2400	2700	...	0	0.00	0	0.00	...
4	1	10	2400	4800	5100	1950	1	0.19	1	0.00	...
5	1	10	4800	9600	9900	2400	2	0.40	1	0.03	...
6	1	40	600	1200	1500	300	1	0.54	1	0.04	...
7	1	40	900	1800	2100	310	2	0.45	1	1.00	...
8	1	40	1200	2400	2700	300	1	0.28	0	0.00	...
9	1	40	2400	4800	5100	330	1	0.55	2	0.28	...
10	1	40	4800	9600	9900	320	3	0.55	2	0.55	...
11	1	80	600	1200	1500	...	0	0.00	1	0.20	...
12	1	80	900	1800	2100	620	1	0.34	1	1.00	...
13	1	80	1200	2400	2700	800	1	0.36	2	0.11	...
14	1	80	2400	4800	5100	...	0	0.00	1	0.00	...
15	1	160	4800	9600	9900	1140	2	0.57	0	0.00	...
16	1	160	600	1200	1500	...	0	0.00	0	0.00	...
17	1	160	900	1800	2100	780	1	0.16	1	0.24	...
18	1	160	1200	2400	2700	1140	1	0.06	1	0.01	...
19	1	160	2400	4800	5100	2250	1	0.07	2	0.42	...
20	1	160	4800	9600	9900	2080	1	0.59	1	0.01	...
21	1	200	600	1200	1500	...	0	0.00	0	0.00	...
22	1	200	900	1800	2100	...	0	0.00	0	0.00	...
23	1	200	1200	2400	2700	1140	1	0.06	1	0.08	...
24	1	200	2400	4800	5100	700	1	0.77	1	0.00	...
25	1	200	4800	9600	9900	2310	1	0.54	1	0.02	...
26	2	12	600	1200	1500	30	1	0.97	1	1.00	0.00
27	2	12	1200	2400	2700	35	1	0.98	0	0.00	0.77
28	2	12	4800	9600	9900	20	1	1.00	2	0.76	0.27
29	2	60	600	1200	1500	70	1	0.98	1	0.48	0.00

Continuation of Table II											
Test	Species	t_a	t_b	t_c	t_d	t_{cry}	N_{cry}	I_{cry}	N_{jam}	I_{jam}	I_{vol}
...	...	s	s	s	s	s
30	2	60	1200	2400	2700	80	1	0.98	1	0.55	0.37
31	2	60	4800	9600	9900	80	1	1.00	1	0.75	0.60
32	2	240	600	1200	1500	280	1	0.89	1	1.00	0.17
33	2	240	1200	2400	2700	275	1	0.96	2	0.75	0.72
34	2	240	400	9600	9900	270	1	0.99	1	1.00	0.07
35	2	300	600	1200	1500	350	1	0.83	2	0.85	0.23
36	2	300	1200	2400	2700	340	1	0.96	2	0.60	0.27
37	2	300	4800	9600	9900	332	1	0.99	1	1.00	0.12
38	3	50	600	1500	1800	90	1	0.93	1	1.00	...
39	3	50	1200	2700	3000	96	1	0.96	1	1.00	...
40	3	50	4800	9900	10200	120	1	0.99	1	1.00	...

III. RESULTS AND DISCUSSION

A general picture of our experimental observations can be summarized as follows. After decreasing the water flow from the velocity U_a to U_b , for different deceleration times t_a , the velocity U_b , still higher than U_{if} , was sustained for an interval $t_b - t_a$. In these conditions, for most of cases, grains became organized in a lattice structure filling the tube cross section, where grains were trapped though with small fluctuations (microscopic motions¹²). These structures were initially localized and grew along time, in a similar manner as happens in phase transitions and glass formation, and in some cases they appeared and disappeared more than once. The time for the beginning of crystallization, t_{cry} , the number of times crystallization appeared, and their intensity, defined as $I_{cry} = \Delta t_{cry} / (t_b - t_a)$, where Δt_{cry} is the duration of crystallization, are shown in Tab. II. After $\Delta t_1 = t_b - 0$, the liquid velocity was increased to U_c and was sustained for an interval $\Delta t_2 = t_c - t_b$. Under these conditions, for most of cases, jamming occurred, where grains became completely blocked and their microscopic motion disappeared. As with crystallization, jamming appeared and disappeared more than once in some instances. The number of times that

jamming appeared, N_{jam} , and their intensity, defined as $I_{jam} = \Delta t_{jam}/\Delta t_2$, where Δt_{jam} is the duration of jamming, are presented in Tab. II. Finally, at t_c the water velocity was increased to U_d and was maintained for $\Delta t_3 = t_d - t_c$. For species 1, the bed fluidized again, but for species 2 a new crystallization occurred, with grains being organized in a volcano-like lattice, where grains were organized in a static structure in contact with the tube wall while absent in the center of the tube cross section, forming an annular structure. The intensity of the volcano-like structure, defined as $I_{vol} = \Delta t_{vol}/\Delta t_3$, where Δt_{vol} is the duration of the volcano, is also shown in Tab. II. For species 3, the bed remained jammed and it was necessary a higher velocity to unjam it (not shown here). The bed structure and the behavior of individual grains are analyzed and discussed next. Movies of one of our experiments are available as Supplementary Material, and movies and images of several experiments, as well as the numerical scripts used for image processing, are available in Mendeley Data¹⁹.

A. Macroscopic observations

We investigated the evolution of the bed structure by comparing consecutive movie frames along time, for three stages of bed evolution, namely Δt_1 , Δt_2 and Δt_3 . In order to visualize macroscopically the different bed structures, we placed sequences of snapshots side by side, as can be seen in Figs. 4, 5 and 6 for tests 1, 26 and 27, respectively (Tab. II). These figures consist basically in spatiotemporal plots without filtering, since they are constructed directly with unprocessed images. In Figs. 4 to 6, the time between frames was increased in order to enable them to fit the page while showing macroscopically the bed structures.

In Figs. 4 to 6 we observe initially a decrease in the bed height due to the decelerating flow, with the occurrence of crystallization after the velocity U_b was attained. During Δt_2 , with $U_c > U_b$, we observe jamming in Figs. 4 and 5, with grains maintaining their respective positions along frames, but not in Fig. 6. Finally, during Δt_3 we observe fluidization again in Fig. 4, jamming in Fig. 5, and a volcano-like structure in Fig. 6. The formation of the volcano-like structure is shown in more detail in Fig. 7, and can be better observed in one of the movies available as Supplementary Material¹⁹, corresponding to test 29 (Tab. II), and in snapshots of other cases, available in Mendeley Data¹⁹.

Based on image processing of all experiments, we identified the different structures and their respective durations, which are shown in Tab. II. In addition, we measured the bed heights and

Crystallization and jamming in narrow fluidized beds

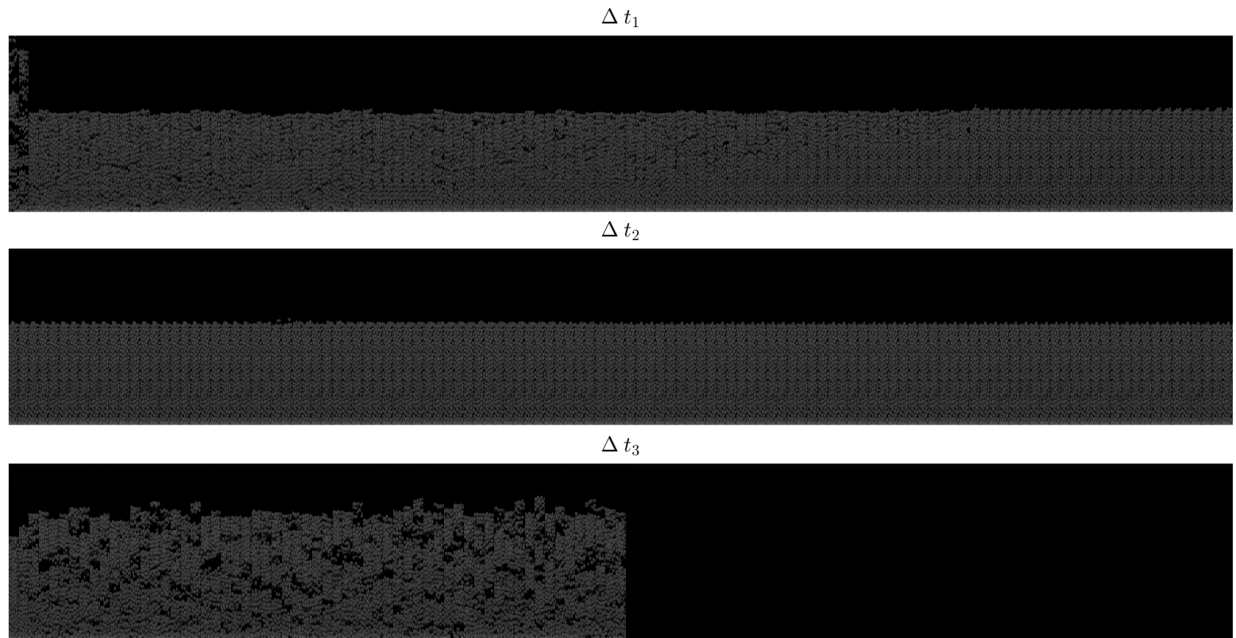


FIG. 4. Snapshots placed side by side for Test 1. The first row corresponds to Δt_1 , the second to Δt_2 and the third to Δt_3 . Time between frames is of 5 s.

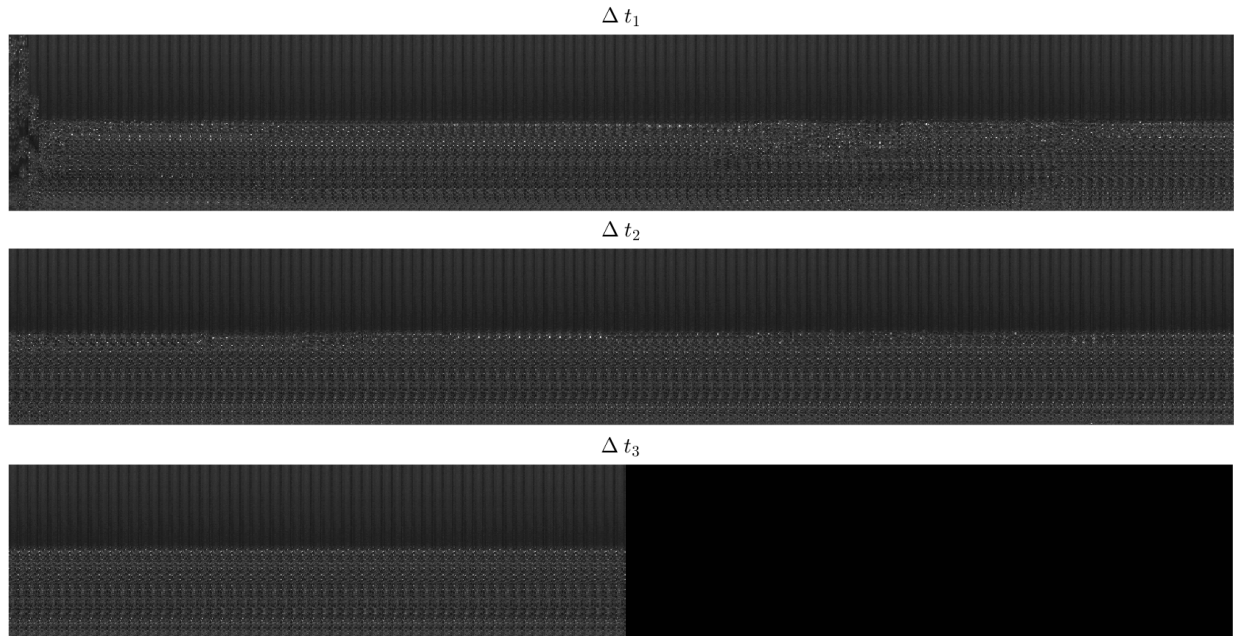


FIG. 5. Snapshots placed side by side for Test 26. The first row corresponds to Δt_1 , the second to Δt_2 and the third to Δt_3 . Time between frames is of 5 s.

obtained the mean particle fraction, computed as the bed volume divided by that of individual

Crystallization and jamming in narrow fluidized beds

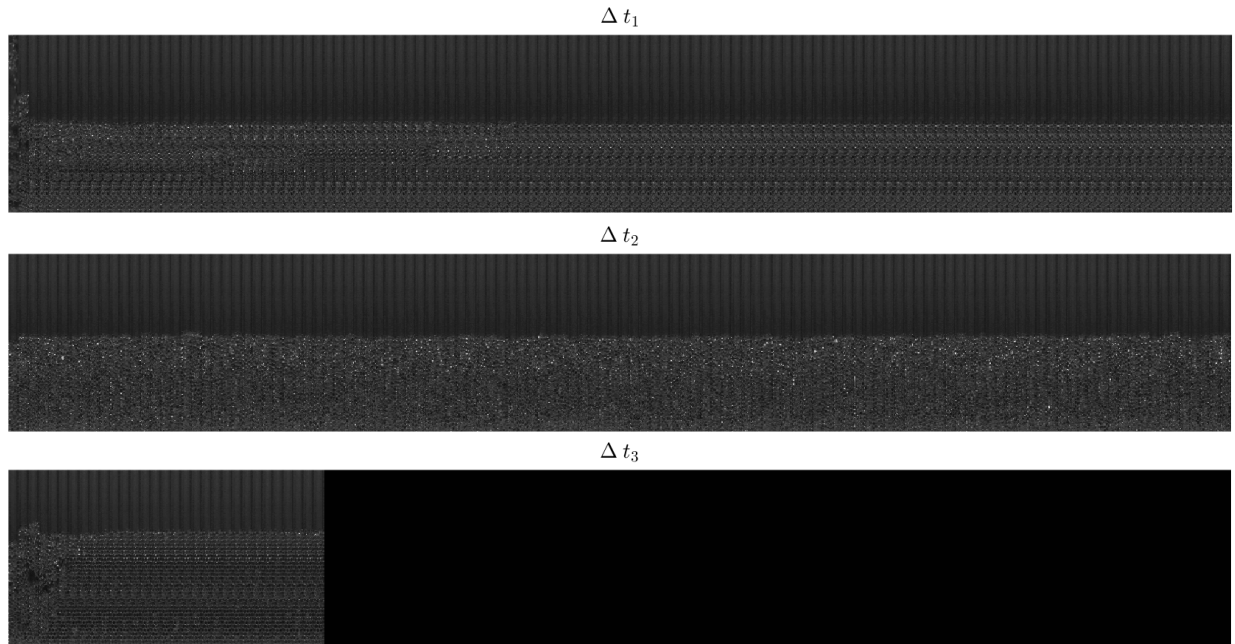


FIG. 6. Snapshots placed side by side for Test 27. The first row corresponds to Δt_1 , the second to Δt_2 and the third to Δt_3 . Time between frames is of 10 s.

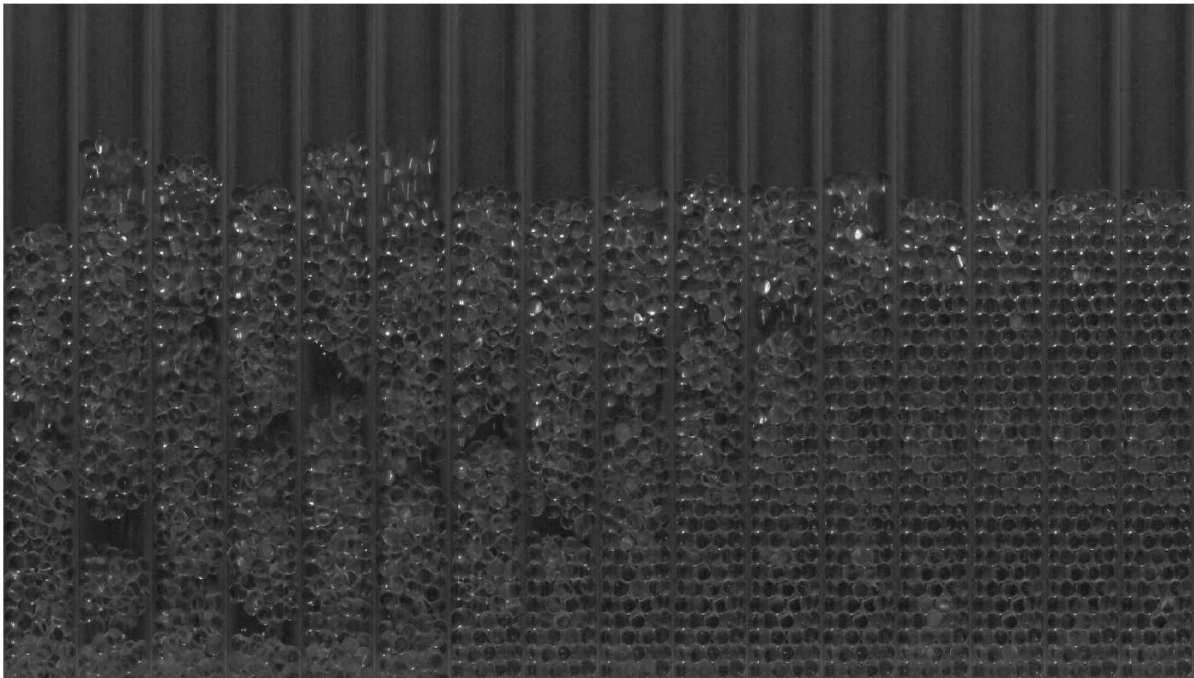


FIG. 7. Snapshots placed side by side for the intervals of Test 27 in which the volcano-like structure is formed. Time between frames is of 5 s.

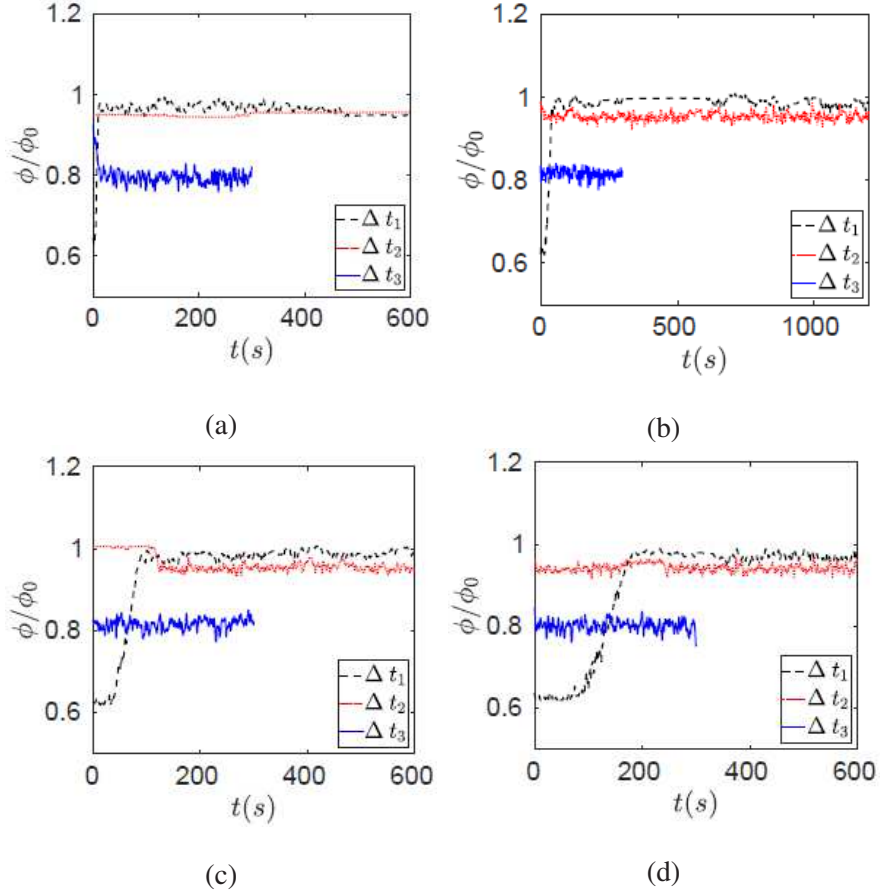


FIG. 8. Evolution of the mean particle fraction along the different intervals. Figures (a), (b), (c) and (d) correspond to tests 1, 8, 11 and 16, respectively. The corresponding intervals are listed in the key.

beads. Figure 8 shows the mean particle fraction normalized by the value corresponding to incipient fluidization, ϕ/ϕ_0 , as a function of time for intervals Δt_1 , Δt_2 and Δt_3 . Figures 8(a), 8(b), 8(c) and 8(d) correspond to tests 1, 8, 11 and 16 (Tab. II), respectively, and represent of the ensemble of behaviors observed in our tests with species 1 and 3 in terms of occurrence of crystallization and jamming.

We observe first that in our tests the particle fractions of crystallized and jammed beds were equal or lower than that of the initial bed, meaning that beds are expanded with respect to incipient fluidization conditions. Then, we observe that, for beds that crystallized, the jammed state maintains approximately the same particle fraction, meaning that the grains basically stopped their microscopic motion when compared with the crystallized condition. Finally, when the water velocity is increased and the bed re-fluidized, the particle fraction decreases. This is the general picture for most tests, but some variations happened. For example, in some few tests, such as test 8, jamming did not occur, and, for that reason, we can observe in Fig. 8(b) that ϕ oscillates and

attains values lower than that of crystallization. In other few cases, such as in test 11, crystallization did not occur but jamming appeared during part of Δt_2 . For these cases, Fig. 8(c) shows that the bed attains a higher value of ϕ during jamming. For other few cases, neither crystallization nor jamming occurred (Fig. 8(d)), and the value of ϕ decreased with the increase of the water velocity. Finally, the most strong variation during Δt_3 was the appearance of a volcano-like structure for species 2. However, given the radial variation of this kind of structure, we understand that the mean void fraction is not a pertinent parameter and we did not compute it. Instead, we analyze that structure in terms of intensity (next).

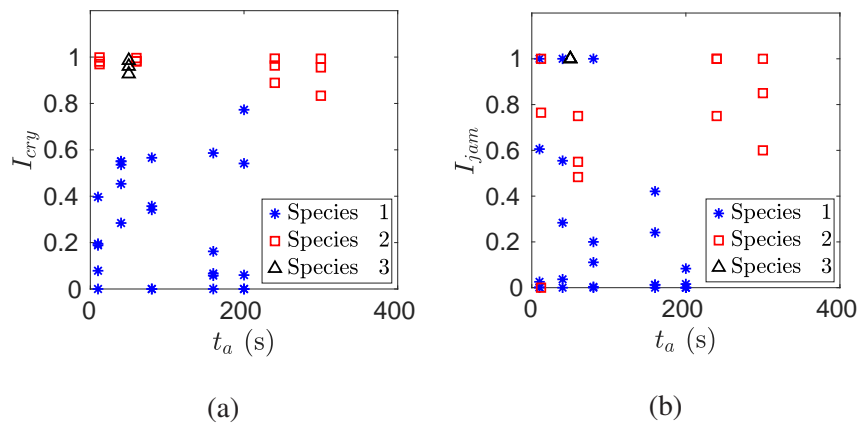


FIG. 9. Intensities of (a) crystallization and (b) jamming as functions of the deceleration time t_a .

As in some tests crystallization and Jamming appeared only once and lasted until the end of intervals Δt_1 and Δt_2 , respectively, while in some others they appeared and disappeared more than once, and in still other tests they did not appear, we measured the total duration of crystallization and jamming and computed their intensities I_{cry} and I_{jam} , respectively. Because in their experiments Goldman and Swinney¹² found that those states depend on the deceleration rate, we investigate next their variation with t_a , Figs. 9(a) and 9(b) showing, respectively, I_{cry} and I_{jam} as functions of the deceleration time t_a . It is remarkable how both the crystallization and jamming intensities do not depend on the deceleration rate, but rather on the grain type: beds consisting of larger and lighter grains tend to be crystallized and jammed. This is in clear contrast with the findings of Goldman and Swinney¹². However, while they used only one grain type and did not investigate the effect of grain size and weight, our beds were much narrower than theirs ($D/d \leq 4.2$ in our case and $D/d \sim 100$ in Goldman and Swinney¹²). Therefore, in the case of very narrow tubes (at least $D/d \leq 5$), the grain characteristics determines the behavior of the bed under de-fluidizing and fluidizing conditions, different from less narrow beds. This is an important

characteristic of highly confined beds that had been unknown until now.

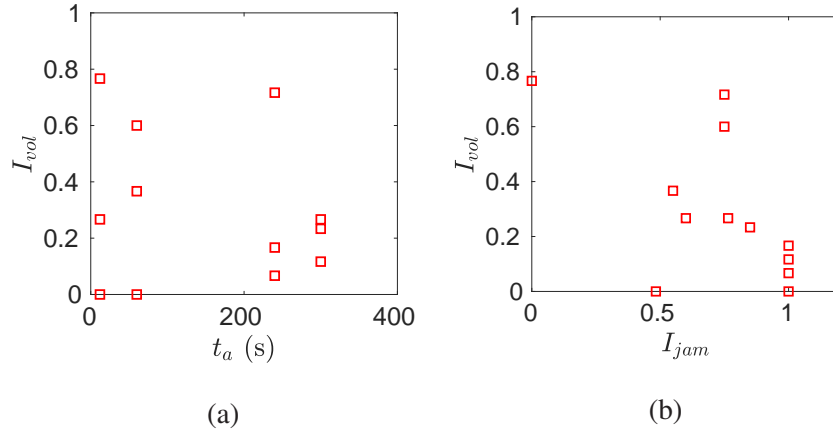


FIG. 10. Intensity of the volcano-like structure as function of (a) the deceleration time t_a and (b) intensity of jamming I_{jam} .

Finally, we computed the intensity of the volcano-like structure appearing for species 2, I_{vol} , and analyzed its behavior as a function of the deceleration time t_a , as shown in Fig. 10(a), but also of the intensity of jamming I_{jam} (once jamming occurred just before the volcano crystallization), as shown in Fig. 10(b). We could find no clear dependence on neither t_a nor I_{jam} . The transition from jamming to the volcano structure is also a characteristic of highly confined beds that had not been reported until now, but it rests to be further investigated.

B. Microscopic observations

In addition to identifying bed structures, we tracked individual grains along movie frames with numerical scripts based on Kelley and Ouellette²⁰ and Houssais et al.²¹. Because the bed was three dimensional, only grains in contact with the tube wall within the field of view of the camera could be tracked. Therefore, measurements were based on a frontal view of a cylindrical plane, which we associated with a Cartesian coordinate system. With the position of tracked grains, we computed their trajectories and obtained two-dimensional displacements and velocities. In order to further investigate the crystallization and jamming processes, we computed the x and y (Fig. 1) components of the instantaneous velocity of each grain, U_p and V_p , respectively, of velocity fluctuations, u_p and v_p , respectively, and the two-dimensional granular temperature θ as in Eq. 1. The velocity fluctuations were computed as the deviation of the instantaneous velocity of each grain from the average value for the ensemble of grains.

$$\theta = \frac{1}{2} (u_p^2 + v_p^2) \quad (1)$$

In addition, we computed a rms average of the norm of the velocity (in the xy plane), as in Eq. 2,

$$V_{rms} = \sqrt{\sum_{i=1}^N \frac{1}{N} (U_p)^2 + \sum_{i=1}^N \frac{1}{N} (V_p)^2} \quad (2)$$

where V_{rms} is the instantaneous rms average for the ensemble of grains, i refers to the i^{th} grain, and N is the number of considered grains (appearing in the image). Figures 11(a), 11(b), 11(c) and 11(d) present V_{rms} for tests 1, 8, 11 and 16, respectively.

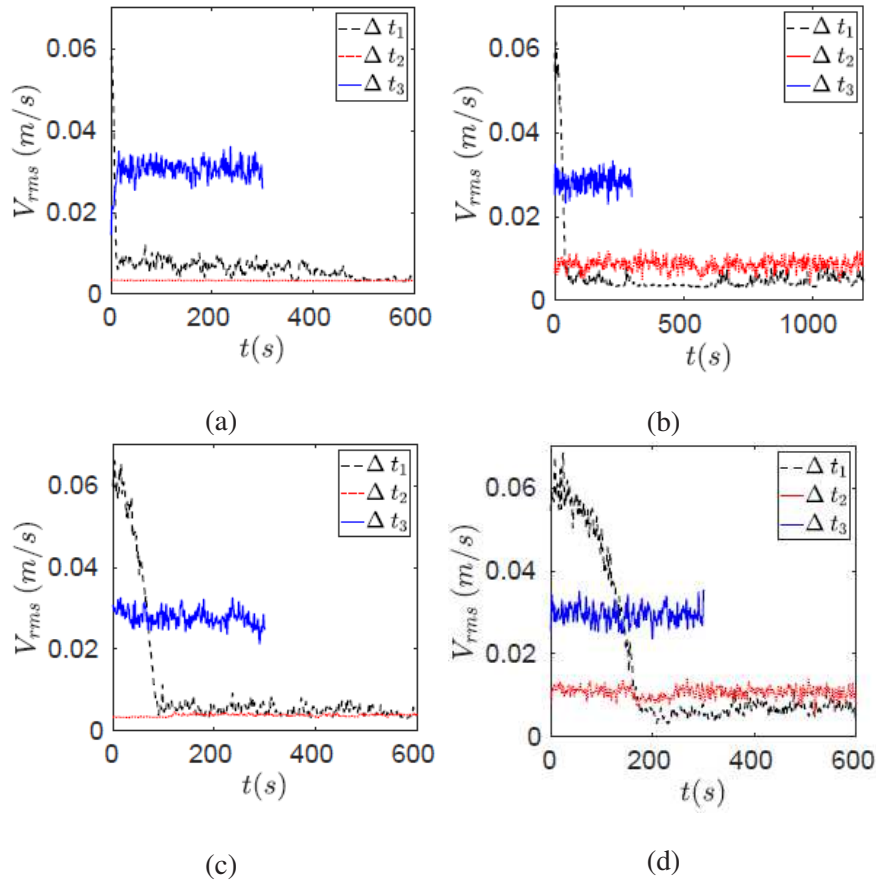


FIG. 11. Evolution of the rms average of the norm of the velocity for all particles along the different intervals. Figures (a), (b), (c) and (d) correspond to tests 1, 8, 11 and 16, respectively. The corresponding intervals are listed in the key.

The rms average of the norm of the velocity indicates the degree of microscopic motion of grains, as can be observed in Fig. 11. At the beginning, when bed is fluidized, we observe large values of V_{rms} , which in their turn fluctuate around a mean value. For the initial velocity U_a , the

mean value of V_{rms} is approximately 0.06 m/s. At U_b , values are much smaller, around 0.006 m/s, but still with fluctuations around a mean value, and, when the bed crystallizes, fluctuations of V_{rms} are considerably reduced. When the water velocity is increased to U_c , V_{rms} is still reduced to values around 0.003 m/s if jamming occurs, and fluctuations of V_{rms} virtually disappear. In cases where fluidization occurs, both the value of V_{rms} and its fluctuations increase. When the water velocity reaches U_d , the bed fluidizes and V_{rms} fluctuates around 0.03 m/s.

Based on the two-dimensional granular temperatures (Eq. 1), we estimated the instantaneous values of cross-sectional averages by computing horizontal averages of θ for each frame. Figures 12(a), 12(b), 12(c) and 12(d) show spatio-temporal diagrams of cross-sectional averages of the granular temperature for tests 1, 8, 11 and 16, respectively, during Δt_1 , where crystallization occurred for some tests. We plotted $10\log\theta$ instead of θ in order to accentuate differences. For all cases, we note initially a rapid decrease in θ , during the deceleration, and then lower values for the cases where crystallization occurred, Figs. 12(a) and 12(b). Of particular interest is the fact that θ reaches lower values first at the bottom of the bed, where crystallization appears first, and those lower values spread upwards as crystallization propagates toward the top, as can be seen in Figs. 12(a) and 12(b) considering their respective t_{cry} . Animations showing the time evolution of the distribution of θ within the bed are available as Supplementary Material and in Mendeley Data¹⁹.

Figures 13(a), 13(b), 13(c) and 13(d) show spatio-temporal diagrams of cross-sectional averages of the granular temperature for tests 1, 8, 11 and 16, respectively, during Δt_2 , where jamming occurred for some tests. We note the much lower values of θ during jammings, reflecting small level of microscopic motion in the jammed state.

We found that for velocities slightly higher than U_{if} the bed can crystallize, being organized in a static lattice of high compactness without macroscopic motion. While we found that crystal structures are initially localized and grow along time, in a similar manner as happens in phase transitions, we did not find any dependence on the decreasing rate, as found by Goldman and Swinney¹². According to Goldman and Swinney¹², both the local growth and rate dependence would have similarities with glass formation in fluids, where the role of fluid velocity is associated to that of temperature. Jamming usually appears when the crystallized bed is forced upwards by submitting it to a fluid velocity slightly higher than that for crystallization, with grains that are already packed together being forced against each other. Given the high confinement of narrow beds, they become in closer contact with each other and with the tube wall and the microscopic motion vanishes. Previous works have associated jamming in grains with glass formation^{22,23},

Crystallization and jamming in narrow fluidized beds

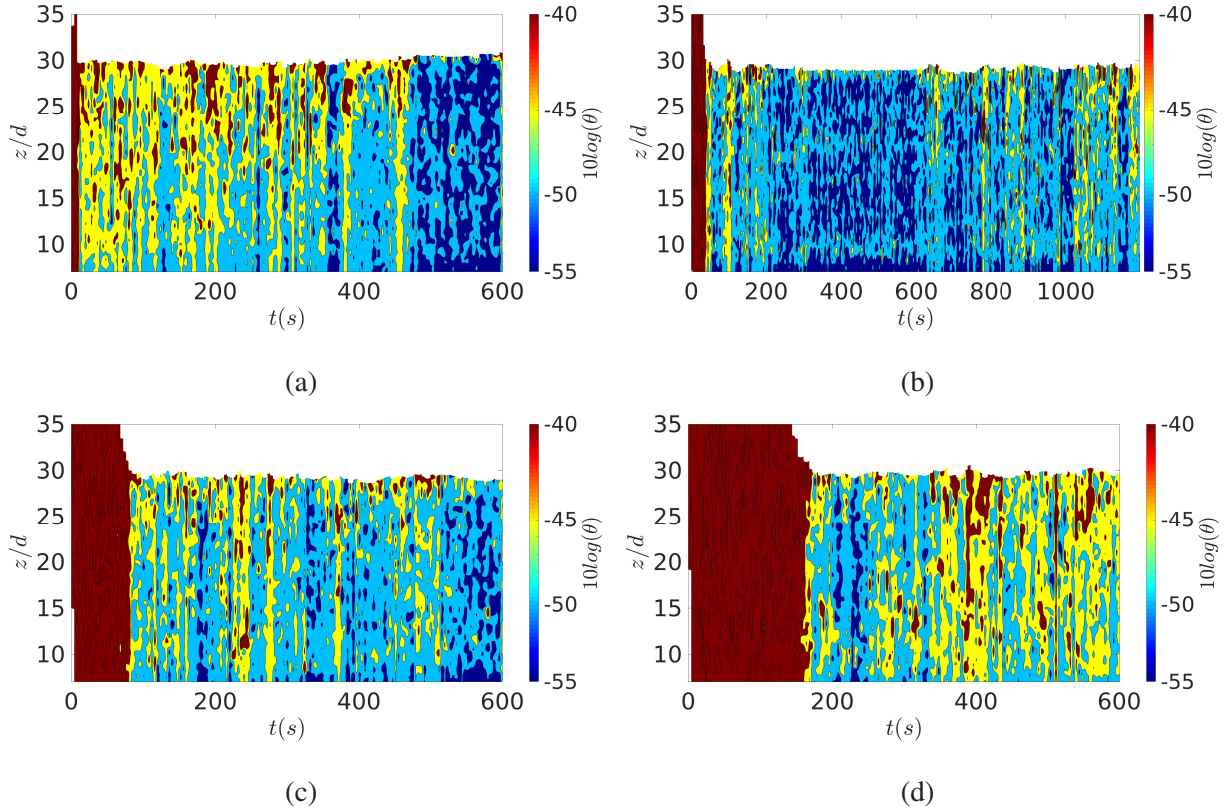


FIG. 12. Spatio-temporal diagrams of cross-sectional averages of the granular temperature during Δt_1 . Figures (a), (b), (c) and (d) correspond to tests 1, 8, 11 and 16, respectively. The corresponding temperatures are listed in the key.

where a glass state is formed by cooling a liquid below its freezing point (supercooled liquid) until solidification (glass) occurs, usually obtained by using high cooling rates, which avoid crystallization below the freezing point and make the liquid viscosity increase drastically so that it becomes a glass below the glass transition temperature. Therefore, the similarity between glass and jamming would be particularly interesting in cases where crystallization does not occur but jamming does; however, this remains to be investigated further.

Finally, crystallization and jamming raise questions concerning the fluidization of narrow beds. In most of cases, for velocities above that for incipient fluidization, our experiments showed that, after being fluidized, beds crystallized and jammed, the latter having static conditions even at the grain scale. Therefore, in the case highly confined beds, considerations about crystallization and jamming should be taken into account in determining fluidization conditions.

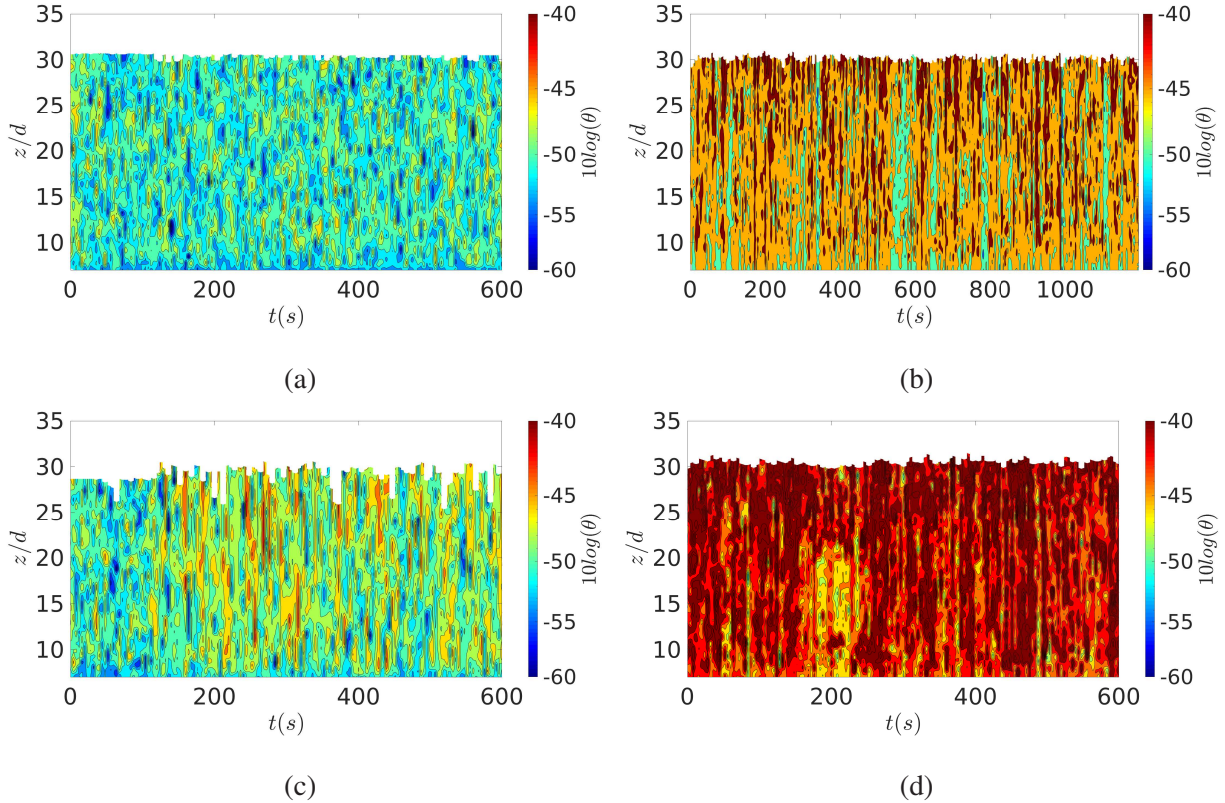


FIG. 13. Spatio-temporal diagrams of cross-sectional averages of the granular temperature during Δt_2 . Figures (a), (b), (c) and (d) correspond to tests 1, 8, 11 and 16, respectively. The corresponding temperatures are listed in the key.

IV. CONCLUSIONS

In this paper we investigated the crystallization and jamming happening at liquid velocities higher than that assuring incipient fluidization in solid-liquid fluidized beds (SLFBs). We were interested in the case of very narrow tubes (ratio between the tube and grain diameters smaller than 5), for which confinement effects are high, and we varied the grain types, water velocities, resting times, and velocity decelerations. We found that, after a decelerating water flow that reached a velocity still higher than that necessary for bed fluidization, grains crystallized in most cases, i.e., became organized in lattice structures occupying the entire tube cross section, where they were trapped though with small fluctuations (microscopic motion). After a certain time, when the liquid velocity was slightly increased, jamming occurred, with microscopic motion disappearing.

We found that both the crystallization and jamming intensities do not depend on the deceleration rate, but rather on the grain type. These findings are in clear contrast with those of Goldman

Crystallization and jamming in narrow fluidized beds

and Swinney¹², who found that the final state depends on the decreasing rate. Our results show that, for very narrow beds, the grain characteristics determines the bed behavior under defluidizing and slight fluidizing conditions. This is an important characteristic of highly confined beds that had been unknown until now.

Finally, we showed that the crystal structures are initially localized and grow along time, in a similar manner as happens in phase transitions, and that a second structure may appear in some cases with a volcano-like form. However, the conditions for the appearance of the latter were not identified and need to be investigated further. Our findings raise the question of fluidization conditions, which should take into consideration crystallization and jamming in the case of highly confined beds.

SUPPLEMENTARY MATERIAL

See Supplementary Material for microscopy images of the used grains, instantaneous snapshots of particle positions for tests 1, 8, 11 and 16, movies showing the evolution of a fluidized bed, and animations showing the distribution of granular temperature.

DATA AVAILABILITY

The data that support the findings of this study are openly available in Mendeley Data¹⁹ at <http://dx.doi.org/10.17632/j28vhs37n8.1>.

ACKNOWLEDGMENTS

Fernando David Cúñez is grateful to FAPESP (Grant Nos. 2016/18189-0 and 2018/23838-3), and Erick Franklin would like to express his gratitude to FAPESP (Grant No. 2018/14981-7) and to CNPq (Grant No. 400284/2016-2) for the financial support they provided.

REFERENCES

- ¹F. D. Cúñez and E. M. Franklin, “Mimicking layer inversion in solid-liquid fluidized beds in narrow tubes,” *Powder Technol.* **364**, 994–1008 (2020).

- ²T. B. Anderson and R. Jackson, “A fluid mechanical description of fluidized beds. Comparison of theory and experiment,” *Ind. Eng. Chem. Fundamen.* **8**, 137–144 (1969).
- ³M. M. El-Kaissy and G. M. Homsy, “Instability waves and the origin of bubbles in fluidized beds: Part 1: Experiments,” *Int. J. Multiphase Flow* **2**, 379 – 395 (1976).
- ⁴A. K. Didwania and G. M. Homsy, “Flow regimes and flow transitions in liquid fluidized beds,” *Int. J. Multiphase Flow* **7**, 563–580 (1981).
- ⁵R. Zenit, M. L. Hunt, and C. E. Brennen, “Collisional particle pressure measurements in solid-liquid flows,” *J. Fluid Mech.* **353**, 261–283 (1997).
- ⁶R. Zenit and M. L. Hunt, “Solid fraction fluctuations in solid-liquid flows,” *Int. J. Multiphase Flow* **26**, 763 – 781 (2000).
- ⁷P. Duru, M. Nicolas, J. Hinch, and É. Guazzelli, “Constitutive laws in liquid-fluidized beds,” *J. Fluid Mech.* **452**, 371–404 (2002).
- ⁸P. Duru and É. Guazzelli, “Experimental investigation on the secondary instability of liquid-fluidized beds and the formation of bubbles,” *J. Fluid Mech.* **470**, 359–382 (2002).
- ⁹A. Aguilar-Corona, R. Zenit, and O. Masbernat, “Collisions in a liquid fluidized bed,” *Int. J. Multiphase Flow* **37**, 695 – 705 (2011).
- ¹⁰S. V. Ghatage, Z. Peng, M. J. Sathe, E. Doroodchi, N. Padhiyar, B. Moghtaderi, J. B. Joshi, and G. M. Evans, “Stability analysis in solid-liquid fluidized beds: Experimental and computational,” *Chem. Eng. J.* **256**, 169 – 186 (2014).
- ¹¹F. D. Cúñez and E. M. Franklin, “Plug regime in water fluidized beds in very narrow tubes,” *Powder Technol.* **345**, 234–246 (2019).
- ¹²D. I. Goldman and H. L. Swinney, “Signatures of glass formation in a fluidized bed of hard spheres,” *Phys. Rev. Lett.* **96**, 145702 (2006).
- ¹³A. Tariot, G. Gauthier, and P. Gondret, “Granular compaction by fluidization,” *EPJ Web Conf.* **140** (2017), 10.1051/epjconf/201714010003.
- ¹⁴G. Gauthier and P. Gondret, “Compaction of liquid immersed granular packings by small upward flows,” *Phys. Rev. Fluids* **4**, 074308 (2019).
- ¹⁵G. Jin, Y. Nie, and D. Liu, “Numerical simulation of pulsed liquid fluidized bed and its experimental validation,” *Powder Technol.* **119**, 153–163 (2001).
- ¹⁶A. Rao, J. S. Curtis, B. C. Hancock, and C. Wassgren, “The effect of column diameter and bed height on minimum fluidization velocity,” *AIChE J.* **56**, 2304–2311 (2010).

- ¹⁷O. L. do Nascimento, D. A. Reay, and V. Zivkovic, “Influence of surface forces and wall effects on the minimum fluidization velocity of liquid-solid micro-fluidized beds,” *Powder Technol.* **304**, 55–62 (2016).
- ¹⁸X. Li, M. Liu, and Y. Li, “Hydrodynamic behavior of liquid–solid micro-fluidized beds determined from bed expansion,” *Particuology* **38**, 103–112 (2018).
- ¹⁹F. D. Cúñez and E. M. Franklin, “Matlab scripts for processing and post-processing experimental data for ‘Crystallization and jamming in narrow fluidized beds’,” *Mendeley Data* (2020), <http://dx.doi.org/10.17632/j28vhs37n8.1>.
- ²⁰D. H. Kelley and N. T. Ouellette, “Using particle tracking to measure flow instabilities in an undergraduate laboratory experiment,” *Am. J. Phys.* **79**, 267–273 (2011).
- ²¹M. Houssais, C. P. Ortiz, D. J. Durian, and D. J. Jerolmack, “Onset of sediment transport is a continuous transition driven by fluid shear and granular creep,” *Nat. Commun.* **6** (2015).
- ²²A. J. Liu and S. R. Nagel, “Jamming is not just cool any more,” *Nature* **396**, 21–22 (1998).
- ²³C. S. O’Hern, S. A. Langer, A. J. Liu, and S. R. Nagel, “Force distributions near jamming and glass transitions,” *Phys. Rev. Lett.* **86**, 111–114 (2001).